NANO LETTERS

Letter

pubs.acs.org/NanoLett

# Waveguide Coupled Resonance Fluorescence from On-Chip Quantum Emitter

Maxim N. Makhonin,*[,†] James E. Dixon,[†] Rikki J. Coles,[†] Ben Royall,[†] Isaac J. Luxmoore,[†] Edmund Clarke,[‡] Maxime Hugues,[‡] Maurice S. Skolnick,[†] and A. Mark Fox[†]

[†]Department of Physics and Astronomy and [‡]EPSRC National Centre for III−V Technologies, University of Sheffield, Sheffield S3 7RH, United Kingdom

Supporting Information

**ABSTRACT:** Resonantly driven quantum emitters offer a very promising route to obtain highly coherent sources of single photons required for applications in quantum information processing (QIP). Realizing this for on-chip scalable devices would be important for scientific advances and practical applications in the field of integrated quantum optics. Here we report on-chip quantum dot (QD) resonance fluorescence (RF) efficiently coupled into a single-mode waveguide, a key component of a photonic integrated circuit, with a negligible resonant laser background and show that the QD coherence is enhanced by more than a factor of 4 compared to off-resonant excitation. Single-photon behavior is confirmed under resonant excitation, and fast fluctuating charge dynamics are revealed in autocorrelation $g^{(2)}$ measurements. The potential for triggered operation is verified in pulsed RF. These results pave the way to a novel class of integrated quantum-optical devices for on-chip quantum information processing with embedded resonantly driven quantum emitters.

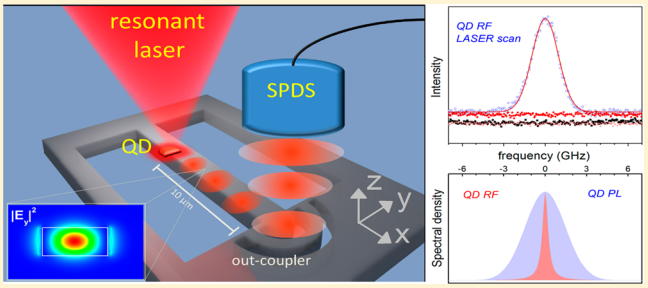


**KEYWORDS:** *Quantum dot, resonance fluorescence, waveguide, integrated quantum optical circuit*

Advances in nanotechnology provide techniques for the realization of integrated quantum-optical circuits for on-chip quantum information processing (QIP).[1−3] Highly coherent, indistinguishable single photons are required for such devices. Such photons[4,5] can be generated by parametric down-conversion[6,7] or from quantum emitters such as color centers[8] and quantum dots[9] (QDs). Among these, semiconductor QDs offer distinctive capabilities including on-demand operation,[10] adiabatic rapid passage,[11] coherent control,[12] frequency tuning,[13] and compatibility with semiconductor nanotechnology that allow fabrication of photonic devices with embedded single photon emitters.

The indistinguishability of single photons is determined by the ratio of the dephasing time $T_2$ to the radiative lifetime $T_1$; close to Fourier-transform-limited coherence with $T_2$ approaching $2T_1$ is required for ideal gate fidelities in QIP applications. This benchmark is not achieved when the dots are excited above the band gap or quasi-resonantly in the p-shell.[10,14,15] On the other hand, the resonant excitation of the fundamental s-shell exciton transition reduces the dephasing[10,15] as a result of the reduction in electrostatic environmental fluctuations and elimination of incoherent phonon assisted relaxation:[10,15,16] hence the coherence of QD photons can be significantly enhanced in resonance fluorescence[15,17−19] (RF). Moreover, resonant excitation combined with RF provides a means for the manipulation and read-out of QD spin-qubit states.[20] RF into free space was first observed from a QD in 2007[21,22] and is now an established technique in several laboratories worldwide. However, the implementation of QD RF in scalable on-chip geometries has so far not been achieved.

In this work we report the experimental observation of resonance fluorescence from a QD coupled efficiently to a single-mode waveguide in a photonic chip. We employ suspended single mode waveguides with high refractive index contrast to provide strong light confinement. Such waveguides have favorable attributes for on-chip quantum optical circuits. They enable low loss transmission of photons around bends of radius less than 2 $\mu$m as required for on-chip components such as beam splitters[23] and more complex circuit architectures, as well as high QD coupling efficiencies in excess of 90% into the waveguide mode[24] (see Supporting Information, Figure S2). The waveguide geometry also provides a ready-made means to separate stray laser photons from the RF: the RF photons propagate perpendicular to the laser allowing the excitation and collection spots to be spatially separated. Moreover, the polarization of the excitation laser can be set to be orthogonal to the one supported by the waveguide, which further suppresses the laser photons. However, in practice the presence of etched surfaces may cause stray laser scattering that may in

**Received:** August 27, 2014
**Revised:** November 4, 2014
**Published:** November 10, 2014

   dx.doi.org/10.1021/nl5032937 | *Nano Lett.* 2014, 14, 6997−7002

turn obscure the RF signal, which may explain why on-chip RF has not been observed before.

The structure we use consisted of a single self-assembled InGaAs quantum dot embedded within a single-mode, suspended vacuum-clad GaAs waveguide with an out-coupler at its end for efficient photon extraction.[25] (See sample details in the Methods section.) The dot was selected from within a QD ensemble of density ~$10^9$ $cm^{-2}$. The QD was excited resonantly by a tunable single-frequency diode laser, and the RF was detected by a single-photon-detection-system (SPDS) after propagating ~10 $\mu$m along the single-mode waveguide to the out-coupler, as shown schematically in Figure 1. The

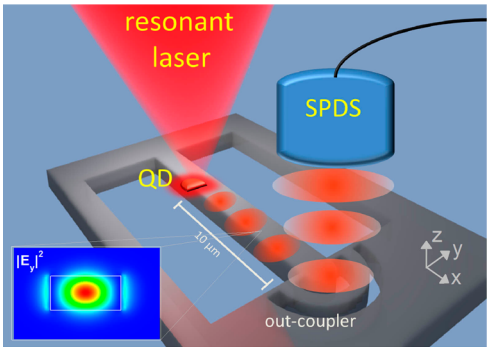


**Figure 1.** Experimental scheme for observing QD resonance fluorescence in a waveguide. The QD is located in a single-mode waveguide and couples only to the TE mode polarized along the y direction. The calculated $|E_y|^2$ intensity profile is shown in the inset. (See Supporting Information.) The laser is polarized along the axis ($x$) orthogonal to the TE mode and is tuned to resonance with the QD exciton transition. The laser excites electron–hole dipoles oriented in the $xy$-plane, and RF photons generated in the dot are guided by the waveguide toward the out-coupler, where they are collected into a single-photon detection system (SPDS). The cross-polarization of the excitation laser and the waveguide strongly suppresses the stray laser photons scattered from the structure. A detailed schematic of the experimental setup is given in the Supplementary Figure S1b.

suppression of the stray laser resonant light by both the intrinsic geometry and the polarization filtering enabled an RF signal to laser background ratio of $S/B \sim 10^2$ to be achieved. In this way we have been able to detect antibunched RF photons with enhanced coherence when using a continuous wave (CW) laser and triggered single RF photon operation with a pulsed laser.

Figure 2 shows the RF signal detected from the QD under scanning resonant CW excitation, together with background contributions recorded separately. The CW RF results presented were made in the low power RF regime well below the Mollow triplet domain,[18,21] i.e., below saturation (Rabi frequency $\Omega \approx 0.5$ GHz $< \Omega_{SAT} \approx 1/\sqrt{2}T_1 \approx 0.6$ GHz). A weak nonresonant laser was applied to stabilize the dot (see Methods), and the resonant laser was slowly scanned repeatedly through the QD fundamental exciton transition as shown in the inset to Figure 2. The resulting RF signal fitted to a Gaussian function gave a full-width-at-half-maximum (fwhm) $h\Delta\nu \sim 9$ $\mu$eV ($\Delta\nu \sim 2.2$ GHz). The measured peak count rate was ~3500 $s^{-1}$, consistent with the calculated overall coupling efficiency to the waveguide of >90% (Supplementary Sections 2 and 3).

The coherence time $T_2$ extracted from the fwhm was ~240 ps, significantly shorter than the radiative lifetime $T_1 = 1.2 \pm$

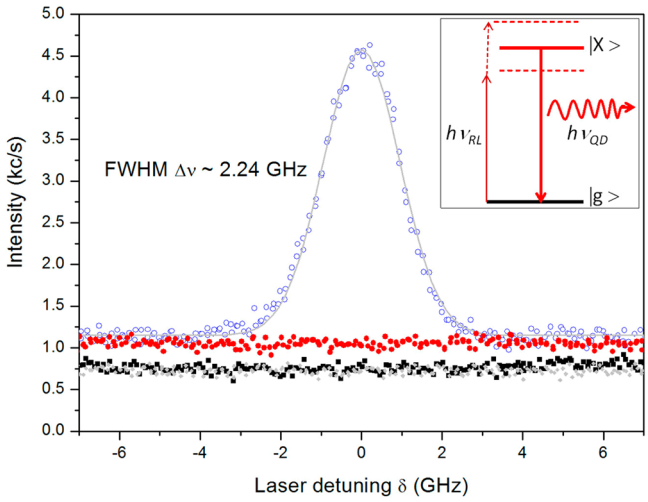


**Figure 2.** QD resonance fluorescence with slow-scanning resonant laser. The QD resonance fluorescence signal plotted as a function of laser detuning $\delta$—blue circles. Background contributions: gray circles—laboratory background mainly due to APD dark counts when both lasers are blocked ($B_{exp}$ ~ 750 c/s); red circles—background $B$ measured when only the nonresonant laser (NRL) is incident on the device ($B = B_{NRL} + B_{exp} \sim 1050$ c/s, $B_{NRL} \sim 300$ c/s); black squares—background measured when only the resonant laser (RL) is incident ($B = B_{RL} + B_{exp}$, $B_{RL} \sim 40$ c/s). The negligible contribution from the resonant laser leads to a high ratio of RF signal to resonant laser background of $S/B_{RL} \sim 90$. The overall signal to background ratio $S/B = S/(B_{RL} + B_{NRL})$ falls to ~10 when both lasers are present, due to the additional background PL photons originating from nonresonant excitation. The latter would be expected to be absent for a QD in a more stable electrostatic environment. The solid line shows a fit to a Gaussian function with inhomogeneous broadening of $\Delta\nu \sim 2.24$ GHz corresponding to a coherence time $T_2 \sim 240$ ps. Inset: Energy-level diagram of the scanning resonant laser experiment.

0.1 ns (see Figure 3c). We attribute the broadening to fluctuations in the QD electrostatic environment that lead to spectral diffusion[26,27] on a time scale faster than the scanning rate of the resonant laser, in agreement with autocorrelation measurements presented below. The smallest linewidth observed for QDs in the bulk of the wafer was ~6 $\mu$eV (~1.5 GHz, $T_2 \sim 365$ ps), which is larger than the best values reported for dots embedded well below the surface (see, e.g., ref 18). In our sample the short distance of ~70 nm to the surface may have an adverse effect on the bulk linewidth, although broadening due to local defects and impurities cannot be ruled out.[28] The approximately 30% smaller $T_2$ time in the waveguide may arise from additional fluctuations introduced by the proximity to the etched surfaces introduced in the fabrication. It should be noted that the adverse effect of slow charge fluctuations can, in principle, be reduced by implementing a fast scanning technique[29] or by locking the QD resonance to an external frequency reference.[30]

The QD coherence was further investigated by using Michelson interferometer techniques. The first-order correlation function $g^{(1)}(\tau)$ is shown in Figure 3a. Under nonresonant excitation, the $g^{(1)}(\tau)$ data fitted to a Gaussian function as expected for inhomogeneous broadening and yielded $T_2 = 154 \pm 5$ ps. Under resonant excitation the $g^{(1)}(\tau)$ data changed to the exponential decay characteristic of homogeneous broadening, and the value of $T_2$ increased by more than four times to $T_2^{RL} = 640 \pm 40$ ps. Fourier transforms of the fitted $g^{(1)}(\tau)$


dx.doi.org/10.1021/nl5032937 | Nano Lett. 2014, 14, 6997–7002

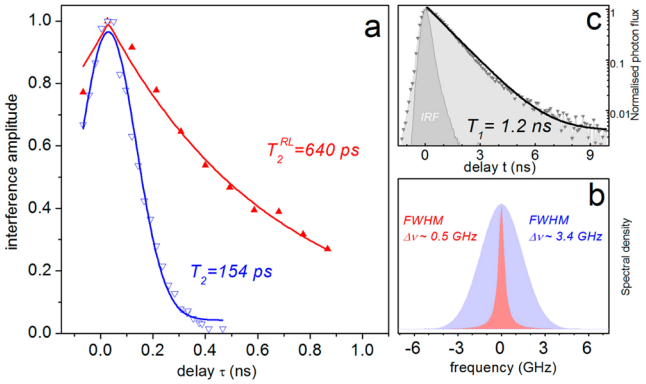


**Figure 3.** QD coherence time. (a) Michelson interferometer fringe amplitude versus time delay $\tau$. The amplitude is proportional to the first order correlation function $g^{(1)}(\tau)$. The blue and red data points correspond respectively to nonresonant excitation and resonant excitation with detuning $\delta \approx 0$. The nonresonant laser power $P_{NRL}$ was $\sim 0.5P_{SAT}$, while the resonant laser power was maintained in the low power RF regime[18,21] ($\Omega \approx 0.4$ GHz $< \Omega_{SAT} \approx 1/\sqrt{2}T_1 \approx 0.6$ GHz). Blue curve—Gaussian fit with $T_2 = 154 \pm 5$ ps. Red curve—exponential fit with $T_2^{RL} = 640 \pm 40$ ps. (b) Fourier transform of the $g^{(1)}(\tau)$ functions from (a) calculated from the fitted curves. Light blue and light red correspond respectively to nonresonant and resonant excitation and have linewidths $h\Delta\nu$ of ~14 $\mu$eV ($\Delta\nu \sim 3.4$ GHz) and ~2 $\mu$eV ($\Delta\nu \sim 0.5$ GHz).[31] (c) Lifetime measurement data—light gray points. Dark gray curve—APD instrument response function with fwhm ~400 ps. Black curve—exponential fit with $T_1 = 1.2 \pm 0.1$ ns.

functions are plotted in Figure 3b. A clear transition from inhomogeneous broadening (Gaussian linewidth with $h\Delta\nu \sim 14$ $\mu$eV, $\Delta\nu \sim 3.4$ GHz) under nonresonant pumping to homogeneous broadening (Lorentzian linewidth with $h\Delta\nu \sim 2$ $\mu$eV, $\Delta\nu \sim 0.5$ GHz) under resonant excitation is observed.[31]

The slightly larger linewidth in Figure 3b under nonresonant excitation compared to the scanning RF experiment in Figure 2 suggests that the additional carriers associated with such excitation cause additional broadening due to increased charge fluctuations. However, the main point is that when the laser is tuned to resonance with the QD, a substantial increase in the coherence time is observed. In these conditions, the ratio of coherent photons to the total signal emitted by the QD is given by $T_2/2T_1$.[17] Pure dephasing processes on a time scale $T_2^*$ limit the coherence through $T_2^{-1} = (2T_1)^{-1} + (T_2^*)^{-1}$. The value of $T_1$ was determined by time-resolved photoluminescence measurements to be $1.2 \pm 0.1$ ns (see Figure 3c), which implies that the coherent ratio in our experiment was ~27%, and the pure dephasing time $T_2^*$ calculated was ~870 ps. The significant enhancement of the coherence is a key advantage of using RF photons; coherence times limited only by the laser itself should ultimately be achievable in the $T_2 = 2T_1$ Fourier limit from a dot with a smaller linewidth.[18,19]

Hanbury Brown and Twiss (HBT) measurements were performed to investigate the statistics of the RF photons. The two-photon correlation function $g^{(2)}(\tau)$ was first measured for the QD exciton photoluminescence (PL) generated by nonresonant excitation with power $P_{NRL}$ close to the saturation level $P_{SAT}$ (see Figure 4a). A clear antibunching dip was observed with a fitted value of $g^{(2)}(0) < 0.04$ after background subtraction (Supplementary Section 4). The antibunching dip fitted well to the same radiative lifetime of $T_1 = 1.2$ ns determined from time-resolved PL (see Figure 3c). The low value of $g^{(2)}(0)$ confirms the single-photon character of the emission. The HBT experiment was then repeated for the RF photons generated with the laser in resonance with the QD (laser detuning $\delta \approx 0$). Figure 4b displays a more complex behavior with clear antibunching at short times ($\tau < T_1$) and

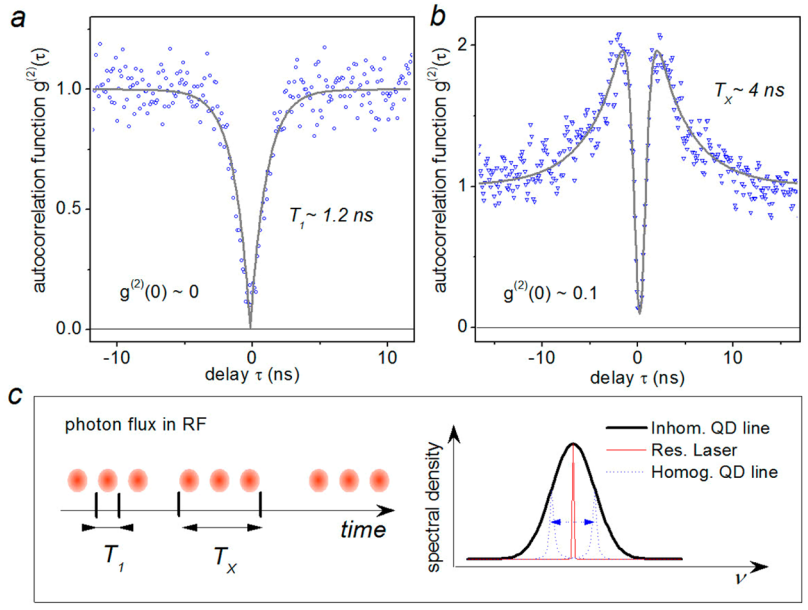


**Figure 4.** Photon statistics in Hanbury Brown and Twiss-type experiments. (a) Autocorrelation function $g^{(2)}(\tau)$ measured for the QD under nonresonant excitation at $P_{NRL} \approx P_{SAT}/2$. (b) Autocorrelation function $g^{(2)}(\tau)$ recorded for resonant excitation in the low RF power regime[18,21] ($\Omega \approx 0.5$ GHz $< \Omega_{SAT} \approx 1/\sqrt{2}T_1 \approx 0.6$ GHz) and $\delta \approx 0$. The data have been normalized after taking account of the background (Supplementary Section 4). (c) Schematic of the spectral diffusion process. Right: dashed (blue) line—lifetime-limited Lorentzian fluctuating within the inhomogeneous broadened Gaussian linewidth shown by the solid (black) line. The thin (red) line corresponds to the resonant laser with fwhm <1 MHz and $\delta \approx 0$. The left diagram displays the photon flux when the homogeneous QD line crosses the laser line, which results in single photons with lifetime $T_1$ and bunches of photons with duration $T_x$.


dx.doi.org/10.1021/nl5032937 | Nano Lett. 2014, 14, 6997−7002

additional bunched shoulders out to ~10 ns. The value of $g^{(2)}(0)$ after correction for background (Supplementary Section 4) was $\approx 0.1 \pm 0.1$, and the decay of the bunching had a characteristic time $T_x \approx 3.8 \pm 0.4$ ns. The bunching observed under resonant excitation cannot be explained by Rabi oscillations or the presence of the weak nonresonant laser (Supplementary Section 4), and we instead attribute it to the spectral diffusion responsible for the broadened line in Figure 2. Figure 4c shows a schematic of the photon flux under resonant excitation when the QD frequency jumps on account of fluctuations in its local environment. The homogeneous QD line moves in and out of resonance with the laser on a time scale $T_x$, leading to the generation of photon bunches on the same time scale.[27,32] The measurement of the RF photon statistics thus provides new insights into the fluctuating QD environment in photonic structures.[33]

To investigate the potential for on-demand operation for the QD single-photon source, we performed RF experiments using a pulsed laser with 9 ps pulse duration and 80 MHz repetition rate (see Methods). The signal emitted from the out-coupler was filtered with a spectrometer and integrated over the QD linewidth while scanning the pulsed laser intensity. Figure 5

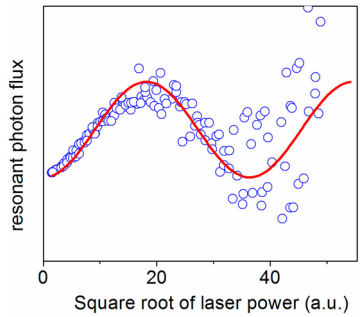


**Figure 5.** Rabi oscillation in resonance fluorescence. Dependence of the QD resonance fluorescence intensity on the excitation amplitude under pulsed resonant excitation. The solid line shows a fit of the data with a sine squared function.[12]

shows Rabi oscillations observed in the RF signal, which demonstrate coherent control of the QD state on a picosecond time scale. The Rabi oscillations observed are similar to previous RF results on QDs,[10,21,22,34,35] but with the clear difference that the single-photon source is integrated within the photonic waveguide and the resonant photons are guided by the waveguide nanostructure for potential implementation in quantum-optical circuits. The usefulness of our present experiments is limited by the high background from the pulsed laser ($S/B \sim 0.8$ for a $\pi$-pulse), but it should be possible to overcome this technical issue by using spectrally narrow pulses[35] and/or photonic cavity on-chip filtering.[36]

The results presented here confirm the potential for using RF from QDs as enhanced coherence single-photon sources in quantum photonic circuits. Moreover, the ability to control the QD frequency in a photonic structure via the Stark effect[13] and lock it to the laser[30] opens a route to building arrays of QDs emitting identical photons into complex quantum photonic circuits. By synchronizing the photons to a pulsed laser,[10,11] on-demand emission should also be possible. At the same time, the issue of spectral diffusion will need to be addressed before all the benefits can be fully realized, as the environmental fluctuations broaden the QD linewidth and hence limit the resonant photon flux. One possible way to reduce these charge fluctuations would be to increase the distance between the QD and the etched surface by redesigning the waveguides with the QDs located in wider taper sections. Optimisation of the crystal growth and device processing are also likely to lead to reduced charge fluctuations.[29]

In future work, a straightforward improvement could be achieved by etching a DBR reflector[37] at one end of the waveguide. This would immediately increase the photon flux by a factor of 2, by reflecting all the waveguide-coupled photons into the required direction. Further improvements could be made by locating the dot in a photonic crystal (PhC) waveguide and using the Purcell effect to increase the radiative rate. Such PhC waveguides offer an alternative approach to micron-scale circuits with high QD coupling efficiencies, although the implementation of sharp bends at short wavelengths (900 nm as opposed to, e.g., 1.55 $\mu$m) requires difficult fabrication.[38] So far in the literature, stray laser scattering in PhC structures is comparable to the RF[20] or even impedes the observation of RF,[39] possibly due to the greater area of etched surfaces in PhCs compared to the suspended waveguides used here. If the issue of stray light could be overcome, then hybrid structures combining slow light PhC waveguides for Purcell enhancement and suspended waveguides for low loss propagation[40] would be a highly promising route forward for QD quantum photonic circuits. At the same time, the application of QD registration techniques[41] or site-controlled QDs[42] would be highly important for the development of scalable devices.

In summary, we have demonstrated a single-photon source integrated into a single-mode waveguide with coherence enhanced by resonant excitation—a key step toward realizing scalable QD-based quantum-optical circuits. The strong light confinement of the suspended GaAs waveguide leads to highly efficient coupling to the QD emitter and enables design of quantum photonic circuits with micron-scale dimensions. The results reveal fast environmental fluctuations on nanosecond time scales that lead to photon bunching due to spectral diffusion. Future work will focus on improvements of the design to reduce the environmental fluctuations and enhance the photon flux, thus enabling ultrabright on-chip single photon sources with a high degree of photon indistinguishability.

**Methods.** *Sample.* The sample we used here was grown by MBE on a GaAs substrate and consisted of a single layer of self-assembled InGaAs QDs embedded at the center of a GaAs layer of thickness 140 nm and grown on top of a $Al_{0.6}Ga_{0.4}As$ sacrificial layer of thickness 1 $\mu$m. The dot density was varied across the wafer by using the rotation-stop technique, permitting the selection of a region of the wafer with a suitable dot density (~$10^9$ cm$^{-2}$). Nanofabrication techniques using electron beam lithography and several etching steps were applied to create suspended, single-mode, rectangular waveguide structures with width, height, and length of 280 nm, 140 nm, and 15 $\mu$m. An out-coupler[25] was incorporated at the end of the waveguide to enable analysis of the RF photons. A scanning electron microscope image of the waveguide nanostructure is given in the Supplementary Figure S1a. The coupling of the QD to the TE waveguide mode reaches 48% for each propagation direction in FDTD simulations (Supplementary Figure S2).

*Experimental Setup.* All measurements were performed in a home-built system composed of a helium bath cryostat at $T$ = 4.2 K with ultrastable positioning control provided by $X,Y,Z$ piezo-stages. The cryostat insert had optical access to the


dx.doi.org/10.1021/nl5032937 | Nano Lett. 2014, 14, 6997−7002

sample in a confocal microscope arrangement. The excitation and collection spots were below 1 $\mu$m in diameter and could be separately moved by more than 10 $\mu$m by scanning mirrors to obtain the exact geometry required for each experiment. For details of the experimental setup see the Supplementary Section 1.

*RF Techniques.* RF signals were only obtained when the sample was simultaneously excited nonresonantly above the GaAs band gap by an additional CW laser operating at 808 nm. The excitation power $P_{NRL}$ was kept well below the saturation power of the QD exciton transition $P_{SAT}$, with typical values of $P_{NRL} \sim P_{SAT}/50$ being used. As previously observed by other groups, this weak nonresonant excitation provides only a small contribution to the total QD signal while helping to keep the QD states stable for resonance fluorescence by reducing the charge fluctuations.[43] The RF signal was detected by an avalanche photodiode after having been filtered through a monochromator in order to remove scattered photons from the nonresonant laser. In this way an overall signal-to-background ratio of $S/B \approx 10$ was typically achieved. The $S/B$ ratio determined by the background from the resonant laser alone was $\approx 90$, but the lower value measured in the RF experiment is caused by the higher background measured when the nonresonant laser is present.

In the Hanbury Brown and Twiss (HBT) experiments, the output of the monochromator was sent to a 50:50 fiber beam splitter connected to two avalanche photodiodes (APDs) and a single-photon counting card. When using above-band excitation, the incoherent QD photoluminescence filtered through the spectrometer was used instead of the RF signal.

In the CW RF experiments, a scanning single-frequency diode laser was used with a scan rate of 400 MHz/s. The scan was repeated several times, and the signal was recorded every 0.5 s. The resonant laser was attenuated to a power level below saturation deduced from RF power dependence measurements[18,21] ($\Omega < \Omega_{SAT} \approx 1/\sqrt{2}T_1 \approx 0.6$ GHz). In the pulsed RF experiments, a femto-second Ti:sapphire laser with a repetition rate of 80 MHz was employed. The pulses were filtered through a pulse shaper to reduce their bandwidth to $\sim$200 $\mu$eV, which corresponds to a pulse duration of $\sim$9 ps. The resonantly emitted photons were collected from the out-coupler and sent to the spectrometer with a CCD detector. The integrated intensity at the QD line was plotted as a function of the optical field amplitude after the residual background from the laser that was linear in power had been subtracted.

## ■ ASSOCIATED CONTENT

### Supporting Information

Additional information and figures. This material is available free of charge via the Internet at http://pubs.acs.org.

## ■ AUTHOR INFORMATION


### Corresponding Author

*E-mail: m.makhonin@sheffield.ac.uk.

### Present Addresses

I.J.L.: College of Engineering, Mathematics and Physical Sciences, University of Exeter, Exeter EX4 4QL, U.K.
M.H.: CNRS CRHEA, F-06560 Valbonne, France.


### Notes

The authors declare no competing financial interest.

## ■ ACKNOWLEDGMENTS

We thank D.N. Krizhanovskii and P. Kok for fruitful discussions. This work has been supported by the EPSRC Programme Grant EP/J007544/1.

## ■ REFERENCES


(1) Knill, E.; Laflamme, R.; Milburn, G. J. A scheme for efficient quantum computation with linear optics. *Nature* **2001**, *409*, 46−52.
(2) O'Brien, J. L.; Furusawa, A.; Vuckovic, J. Photonic quantum technologies. *Nat. Photonics* **2009**, *3*, 687−695.
(3) Kok, P.; Munro, W. J.; Nemoto, K.; Ralph, T. C.; Dowling, J. P.; Milburn, G. J. Linear optical quantum computing with photonic qubits. *Rev. Mod. Phys.* **2007**, *79*, 135−174.
(4) Santori, C.; Fattal, D.; Vuckovic, J.; Solomon, G. S.; Yamamoto, Y. Indistinguishable photons from a single-photon device. *Nature* **2002**, *419*, 594−597.
(5) Gazzano, O.; Michaelis de Vasconcellos, S.; Arnold, C.; Nowak, A.; Galopin, E.; Sagnes, I.; Lanco, L.; Lemaıtre, A.; Senellart, P. Bright solid-state sources of indistinguishable single photons. *Nat. Commun.* **2013**, *4*, 1425.
(6) Silverstone, J. W.; Bonneau, D.; Ohira, K.; Suzuki, N.; Yoshida, H.; Iizuka, N.; Ezaki, M.; Natarajan, C. M.; Tanner, M. G.; Hadfield, R. H.; Zwiller, V.; Marshall, G. D.; Rarity, J. G.; O'Brien, J. L.; Thompson, M. G. On-chip quantum interference between silicon photon-pair sources. *Nat. Photonics* **2014**, *8*, 104−108.
(7) Crespi, A.; Ramponi, R.; Osellame, R.; Sansoni, L.; Bongioanni, I.; Sciarrino, F.; Vallone, G.; Mataloni, P. Integrated photonics quantum gates for polarization qubits. *Nat. Commun.* **2011**, *2*, 566.
(8) Kennard, J. E.; Hadden, J. P.; Marseglia, L.; Aharonovich, I.; Castelletto, S.; Patton, B. R.; Politi, A.; Matthews, J. C. F.; Sinclair, A. G.; Gibson, B. C.; Prawer, S.; Rarity, J. G.; O'Brien, J. L. On-chip manipulation of single photons from a diamond defect. *Phys. Rev. Lett.* **2013**, *111*, 213603.
(9) Gazzano, O.; Almeida, M. P.; Nowak, A.; Portalupi, S. L.; Lemaıtre, A.; Sagnes, I.; White, A. G.; Senellart, P. Entangling Quantum-Logic Gate Operated with an Ultrabright Semiconductor Single-Photon Source. *Phys. Rev. Lett.* **2013**, *110*, 250501.
(10) He, Y.-M.; He, Y.; Wei, Y.-J.; Wu, D.; Atatüre, M.; Schneider, C.; Höfling, S.; Kamp, M.; Lu, C.-Y.; Pan, J.-W. On-demand semiconductor single-photon source with near-unity indistinguishability. *Nat. Nanotechnol.* **2013**, *8*, 213−217.
(11) (a) Simon, C.-M.; Belhadj, T.; Chatel, B.; Amand, T.; Renucci, P.; Lemaitre, A.; Krebs, O.; Dalgarno, P. A.; Warburton, R. J.; Marie, X.; Urbaszek, B. Robust Quantum Dot Exciton Generation via Adiabatic Passage with Frequency-Swept Optical Pulses. *Phys. Rev. Lett.* **2011**, *106*, 166801. (b) Wu, Y.; Piper, I. M.; Ediger, M.; Brereton, P.; Schmidgall, E. R.; Eastham, P. R.; Hugues, M.; Hopkinson, M.; Phillips, R. T. Population Inversion in a Single InGaAs Quantum Dot Using the Method of Adiabatic Rapid Passage. *Phys. Rev. Lett.* **2011**, *106*, 067401.
(12) Ramsay, A. J. A review of the coherent optical control of the exciton and spin states of semiconductor quantum dots. *Semicond. Sci. Technol.* **2010**, *25*, 103001.
(13) Bennett, A. J.; Pooley, M. A.; Cao, Y.; Sköld, N.; Farrer, I.; Ritchie, D. A.; Shields, A. J. Voltage tunability of single-spin states in a quantum dot. *Nature Commun.* **2012**, *4*, 1522.
(14) Kammerer, C.; Voisin, C.; Cassabois, G.; Delalande, C.; Roussignol, Ph.; Klopf, F.; Reithmaier, J. P.; Forchel, A.; Gerard, J. M. Line narrowing in single semiconductor quantum dots: Toward the control of environment effects. *Phys. Rev. B* **2002**, *66*, 041306 (R).
(15) Ates, S.; Ulrich, S. M.; Reitzenstein, S.; Löffler, A.; Forchel, A.; Michler, P. Post-Selected Indistinguishable Photons from the Resonance Fluorescence of a Single Quantum Dot in a Microcavity. *Phys. Rev. Lett.* **2009**, *103*, 167402.
(16) Bennett, A. J.; Unitt, D. C.; Shields, A. J.; Atkinson, P.; Ritchie, D. A. Influence of exciton dynamics on the interference of two photons from a microcavity single-photon source. *Opt. Express* **2005**, *13*, 7772−7778.

(17) Nguyen, H. S.; Sallen, G.; Voisin, C.; Roussignol, Ph.; Diederichs, C.; Cassabois, G. Ultra-coherent single photon source. *Appl. Phys. Lett.* **2011**, *99*, 261904.
(18) Matthiesen, C.; Vamivakas, A. N.; Atatüre, M. Subnatural Linewidth Single Photons from a Quantum Dot. *Phys. Rev. Lett.* **2012**, *108*, 093602.
(19) Matthiesen, C.; Geller, M.; Schulte, C. H. H.; Le Gall, C.; Hansom, J.; Li, Z.; Hugues, M.; Clarke, E.; Atatüre, M. Phase-locked indistinguishable photons with synthesized waveforms from a solid-state source. *Nat. Commun.* **2013**, *4*, 1600.
(20) Carter, S. G.; Sweeney, T. M.; Kim, M.; Kim, C. S.; Solenov, D.; Economou, S. E.; Reinecke, T. L.; Yang, L.; Bracker, A. S.; Gammon, D. Quantum control of a spin qubit coupled to a photonic crystal cavity. *Nat. Photonics* **2013**, *7*, 329−334.
(21) Muller, A.; Flagg, E. B.; Bianucci, P.; Wang, X. Y.; Deppe, D. G.; Ma, W.; Zhang, J.; Salamo, G. J.; Xiao, M.; Shih, C. K. Resonance Fluorescence from a Coherently Driven Semiconductor Quantum Dot in a Cavity. *Phys. Rev. Lett.* **2007**, *99*, 187402.
(22) Kuroda, K.; Kuroda, T.; Watanabe, K.; Mano, T.; Sakoda, K.; et al. Final-state readout of exciton qubits by observing resonantly excited photoluminescence in quantum dots. *Appl. Phys. Lett.* **2007**, *90*, 051909.
(23) Prtljaga, N.; Coles, R. J.; O'Hara, J.; Royall, B.; Clarke, E.; Fox, A. M.; Skolnick, M. S. Monolithic integration of a quantum emitter with a compact on-chip beam-splitter. *Appl. Phys. Lett.* **2014**, *104*, 231107.
(24) Bleuse, J.; Claudon, J.; Creasey, M.; Malik, N. S.; Gerard, J.-M.; Maksymov, I.; Hugonin, J.-P.; Lalanne, P. Inhibition, Enhancement, and Control of Spontaneous Emission in Photonic Nanowires. *Phys. Rev. Lett.* **2011**, *106*, 103601.
(25) Faraon, A.; Fushman, I.; Englund, D.; Stoltz, N.; Petroff, P.; Vuckovic, J. Dipole induced transparency in waveguide coupled photonic crystal cavities. *Opt. Express* **2008**, *16*, 12154.
(26) Houel, J.; Kuhlmann, A. V.; Greuter, L.; Xue, F.; Poggio, M.; Gerardot, B. D.; Dalgarno, P. A.; Badolato, A.; Petroff, P. M.; Ludwig, A.; Reuter, D.; Wieck, A. D.; Warburton, R. J. Probing Single-Charge Fluctuations at a GaAs/AlAs Interface Using Laser Spectroscopy on a Nearby InGaAs Quantum Dot. *Phys. Rev. Lett.* **2012**, *108*, 107401.
(27) Sallen, G.; Tribu, A.; Aichele, T.; André, R.; Besombes, L.; Bougerol, C.; Richard, M.; Tatarenko, S.; Kheng, K.; Poizat, J.-Ph. Subnanosecond spectral diffusion measurement using photon correlation. *Nat. Photonics* **2010**, *4*, 696−699.
(28) De Greve, K.; McMahon, P. L.; Press, D.; Ladd, T. D.; Bisping, D.; Schneider, C.; Kamp, M.; Worschech, L.; Höfling, S.; Forchel, A.; Yamamoto, Y. Ultrafast coherent control and suppressed nuclear feedback of a single quantum dot hole qubit. *Nat. Phys.* **2011**, *7*, 872−878.
(29) Kuhlmann, A. V.; Houel, J.; Ludwig, A.; Greuter, L.; Reuter, D.; Wieck, A. D.; Poggio, M.; Warburton, R. J. Charge noise and spin noise in a semiconductor quantum device. *Nat. Phys.* **2013**, *9*, 570.
(30) Prechtel, J. H.; Kuhlmann, A. V.; Houel, J.; Greuter, L.; Ludwig, A.; Reuter, D.; Wieck, A. D.; Warburton, R. J. Frequency-Stabilized Source of Single Photons from a Solid-State Qubit. *Phys. Rev. X* **2013**, *3*, 041006.
(31) The coherence time $T_2$ obtained from the interference measurement is defined as the time at which the interference amplitude equals 1/e. The fwhm linewidths obtained from the Fourier transform spectra as in Figure 3b have different relation to $T_2$ depending on the broadening mechanism: for Lorentzian $T_2 = 1/\pi\Delta\nu$, for Gaussian $T_2 = 2(\ln 2)^{1/2}/\pi\Delta\nu$.
(32) Ulhaq, A.; Weiler, S.; Ulrich, S. M.; Roßbach, R.; Jetter, M.; Michler, P. Cascaded single-photon emission from the Mollow triplet sidebands of a quantum dot. *Nat. Photonics* **2012**, *6*, 238−242.
(33) Davanco, M.; Hellberg, C. S.; Ates, S.; Badolato, A.; Srinivasan, K. Multiple time scale blinking in InAs quantum dot single-photon sources. *Phys. Rev. B* **2014**, *89*, 161303(R).
(34) Melet, R.; Voliotis, V.; Enderlin, A.; Roditchev, D.; Wang, X. L.; Guillet, T.; Grousson, R. Resonant excitonic emission of a single quantum dot in the Rabi regime. *Phys. Rev. B* **2008**, *78*, 073301.
(35) Schaibley, J. R.; Burgers, A. P.; McCracken, G. A.; Steel, D. G.; Bracker, A. S.; Gammon, D.; Sham, L. J. Direct detection of time-resolved Rabi oscillations in a single quantum dot via resonance fluorescence. *Phys. Rev. B* **2013**, *87*, 115311.
(36) Waks, E.; Vuckovic, J. Dipole Induced Transparency in Drop-Filter Cavity-Waveguide Systems. *Phys. Rev. Lett.* **2006**, *96*, 153601.
(37) Velha, P.; Rodier, J. C.; Lalanne, P.; Hugonin, J. P.; Peyrade, D.; Picard, E.; Charvolin, T.; Hadji, E. Ultra-high-reflectivity photonic-bandgap mirrors in a ridge SOI waveguide. *New J. Phys.* **2006**, *8*, 204.
(38) Asakawa, K.; Sugimoto, Y.; Watanabe, Y.; Ozaki, N.; Mizutani, A.; Takata, Y.; Kitagawa, Y.; Ishikawa, H.; Naoki Ikeda, N.; Awazu, K.; Wang, X.; Watanabe, A.; Nakamura, S.; Ohkouchi, S.; Inoue, K.; Kristensen, M.; Sigmund, O.; Borel, P. I.; Baets, R. Photonic crystal and quantum dot technologies for all-optical switch and logic device. *New J. Phys.* **2006**, *8*, 208.
(39) Englund, D.; Majumdar, A.; Faraon, A.; Toishi, M.; Stoltz, N.; Petroff, P.; Vučković, E. Resonant Excitation of a Quantum Dot Strongly Coupled to a Photonic Crystal Nanocavity. *Phys. Rev. Lett.* **2010**, *104*, 073904.
(40) Vlasov, Y. A.; O'Boyle, M.; Hamann, H. F.; McNab, S. J. Active control of slow light on a chip with photonic crystal waveguides. *Nature* **2005**, *438*, 65−69.
(41) (a) Thon, S. M.; Rakher, M. T.; Kim, H.; Gudat, J.; Irvine, W.T. M.; Petroff, P. M.; Bouwmeester, D. Strong coupling through optical positioning of a quantum dot in a photonic crystal cavity. *Appl. Phys. Lett.* **2009**, *94*, 111115. (b) Kojima, T.; Kojima, K.; Asano, T.; Noda, S. Accurate alignment of a photonic crystal nanocavity with an embedded quantum dot based on optical microscopic photoluminescence imaging. *Appl. Phys. Lett.* **2013**, *102*, 011110.
(42) (a) Jöns, K. D.; Atkinson, P.; Müller, M.; Heldmaier, M.; Ulrich, S. M.; Schmidt, O. G.; Michler, P. Triggered Indistinguishable Single Photons with Narrow Line Widths from Site-Controlled Quantum Dots. *Nano Lett.* **2013**, *13*, 126. (b) Birindelli, S.; Felici, M.; Wildmann, J. S.; Polimeni, A.; Capizzi, M.; Gerardino, A.; Rubini, S.; Martelli, F.; Rastelli, A.; Trotta, R. Single Photons on Demand from Novel Site-Controlled GaAsN/GaAsN:H Quantum Dots. *Nano Lett.* **2014**, *14*, 1275. (c) Huggenberger, A.; Heckelmann, S.; Schneider, C.; Höfling, S.; Reitzenstein, S.; Worschech, L.; Kamp, M.; Forchel, A. Narrow spectral linewidth from single site-controlled In(Ga)As quantum dots with high uniformity. *Appl. Phys. Lett.* **2014**, *98*, 131104. (d) Surrente, A.; Felici, M.; Gallo, P.; Dwir1, B.; Rudra, A.; Biasiol, G.; Sorba, L.; Kapon, E. Ordered systems of site-controlled pyramidal quantum dots incorporated in photonic crystal cavities. *Nanotechnology* **2011**, *22*, 465203. (e) Jamil, A.; Skiba-Szymanska, J.; Kalliakos, S.; Schwagmann, A.; Ward, M. B.; Brody, Y.; Ellis, D. J. P.; Farrer, I.; Griffiths, J. P.; Jones, G. A. C.; Ritchie, D. A.; Shields, A. J. On-chip generation and guiding of quantum light from a site-controlled quantum dot. *Appl. Phys. Lett.* **2014**, *104*, 101108. (f) Yakes, M. K.; Yang, L.; Bracker, A. S.; Sweeney, T. M.; Brereton, P. G.; Kim, M.; Kim, C. S.; Vora, P. M.; Park, D.; Carter, S. G.; Gammon, D. Leveraging Crystal Anisotropy for Deterministic Growth of InAs Quantum Dots with Narrow Optical Linewidths. *Nano Lett.* **2013**, *13*, 4870.
(43) Nguyen, H. S.; Sallen, G.; Voisin, C.; Roussignol, Ph.; Diederichs, C.; Cassabois, G. Optically Gated Resonant Emission of Single Quantum Dots. *Phys. Rev. Lett.* **2012**, *108*, 057401.